

Sea ice as the glacial cycles' climate switch: Role of seasonal and orbital forcing

Hezi Gildor and Eli Tziperman

Environmental Sciences, Weizmann Institute, Rehovot, Israel

Abstract. A box model of the coupled ocean, atmosphere, sea ice, and land ice climate system is used to study glacial-interglacial oscillations under seasonally and orbitally varying solar forcing. The dominant 100 kyr oscillation in land ice volume has the familiar sawtooth shape of climate proxy records, and to zeroth order, it does not depend on the seasonal and Milankovitch forcing. The sea ice controls, via its albedo and insulating effects, the atmospheric moisture fluxes and precipitation that enable the land ice sheet growth. This control and the rapid growth and melting of the sea ice allow the sea ice to rapidly switch the climate system from a growing ice sheet phase to a retreating ice sheet phase and to shape the oscillation's sawtooth structure. A specific physical mechanism is proposed by which the insolation changes act as a pacemaker, setting the phase of the oscillation by directly controlling summer melting of ice sheets. This mechanism is shown to induce deglaciations during periods of lower summer insolation. Superimposed on the 100 kyr are the linear Milankovitch-forced frequencies of 19, 23, and 41 kyr. The transition from 41 kyr glacial cycles to 100 kyr cycles one million years ago may be explained as being due to the activation of the sea ice switch at that time. This would be the case if sea ice extent was more limited during the warmer climate of the early Pleistocene.

1. Introduction

The weakness of the *Milankovitch* [1930] variations in solar radiation at the 100,000 year (100 kyr) timescale has led to the generally accepted conclusion that the glacial-interglacial oscillations at this timescale are most likely not a direct linear response of the climate system to external solar variations [*Imbrie et al., 1992, 1993; Ghil, 1994; Saltzman, 1990*]. In *Gildor and Tziperman* [2000], hereafter called part 1, we described a novel mechanism for glacial oscillations on a timescale of 100 kyr which does not rely on external Milankovitch forcing and which is characterized by the observed asymmetric sawtooth structure of the land ice volume time series (i.e., a slow land ice buildup and a rapid termination). The oscillation mechanism was investigated using a simple, yet explicit zonally averaged box model of the physical climate system, including the ocean (explicitly accounting for the thermohaline circulation), atmosphere, sea ice, and land ice. The proposed mechanism relies on the rapid, switch-like growth and melting of sea ice. The sea ice switches control the hydrological cycle in our model through the sea ice albedo effects and also control the moisture extraction from the ocean, through the insulating effect of a sea ice cover on the air-sea fluxes. Through these two effects the sea ice controls the amount of snow accumulation which enables

the growth of land glaciers and thus switches the climate system from an expanding land glaciers phase to a retreating glacier mode. On the basis of the insight we have obtained into the oscillation mechanism, we were also able to formulate a simple heuristic argument for the 100 kyr timescale (see section 3).

While probably not the direct major forcing of the 100 kyr oscillations, the analysis of proxy observations indicates that the Milankovitch forcing does play a major role in linearly forcing the climate variations on a scale of 23 and 41 kyr as well as in serving as a pacemaker of the 100 kyr cycles [*Imbrie et al., 1992; Saltzman, 1990*]. In this paper therefore we continue the investigation of part 1 by including seasonal solar forcing and then also Milankovitch variations in the solar radiation.

There have been several different proposals as to the way in which Milankovitch forcing affects the 100 kyr glacial cycles. The observed 100 kyr power was explained by *Le Treut and Ghil* [1983] as a nonlinear energy transfer from higher-frequency Milankovitch forcing. *Maasch and Saltzman* [1990], on the other hand, attributed the 100 kyr cycle to a slow CO₂ feedback, without going into its details; in their model, the Milankovitch variations in solar radiation only contribute to the phase locking of the internally driven 100 kyr cycle and to its asymmetric sawtooth structure. *Pailard* [1998] has used a highly simplified model representing the climate system as a set of quasi-steady states driven by the Milankovitch forcing and was able to obtain a good fit to the observed paleoproxy record. He

Copyright 2000 by the American Geophysical Union.

Paper number 1999PA000461.

0883-8305/00/1999PA000461\$12.00

did not attempt, however, to specify the actual physics behind the way the Milankovitch forcing affects the climate system, or the physics responsible for the specified steady states. Climate variability previous to the late Pleistocene's 100 kyr cycles was dominated by a 41 kyr glacial cycle [Raymo, 1998; Birchfield and Ghil, 1993; Saltzman, 1990]. The transition from 41 kyr to 100 kyr was explained as a climate bifurcation due to a gradual increase in overall ice mass [Ghil and Childress, 1987, chapter 12] or due to a slow CO₂ increase by Maasch and Saltzman [1990]. The former authors based their conclusion on the simple coupled model of Ghil and Le Treut [1981], while the latter used an idealized model that does not attempt an explicit representation of some of the physical mechanisms.

In this paper we incorporate a specific way in which the Milankovitch forcing can linearly force a climate response at the 23 and 41 kyr timescales (following Held [1982]) and show that this external Milankovitch forcing indeed leads to a phase locking of the internal 100 kyr climate oscillations. We also propose that the transition from a 41 kyr cycle to a 100 kyr cycle about 700 kyr ago could result from a climate cooling [Ghil and Childress, 1987; Ruddiman and Raymo, 1988; Saltzman and Verbitsky, 1994] which allowed the sea ice cover to expand, activated the sea ice switch mechanism, and started the late Pleistocene 100 kyr glacial cycles. According to this proposal, the 41 kyr oscillations previous to this transition were directly and linearly forced by Milankovitch forcing.

We start in section 2 with a brief description of the model, concentrating on the changes made relative to part 1 in order to accommodate the seasonal and Milankovitch forcing. In section 3 the results obtained using seasonal solar radiation based on today's orbital parameter values are presented, the mechanism of the glacial cycle from part 1 is reviewed in the context of the seasonal model, and the seasonal cycle of key climate variables at different stages of the 100 kyr oscillation is analyzed. Section 4 presents the results of forcing the model with varying orbital parameters. We examine the new variability at 23 and 41 kyr, superimposed on the dominant 100 kyr cycle, as well as the locking of the 100 kyr cycle to the orbital variations. A comparison to a SPECMAP time series [Imbrie et al., 1984] and the transition from a 41 kyr cycle to a 100 kyr cycle about 700 kyr years ago are also discussed. We present our conclusions in section 5.

2. Model Description

The coupled ocean, atmosphere, sea ice, and land ice model (Figure 1) was described in detail in part 1 (the code is available from the authors upon request). For the purpose of the present work, solar forcing was made to vary with season, and in some of the runs the model

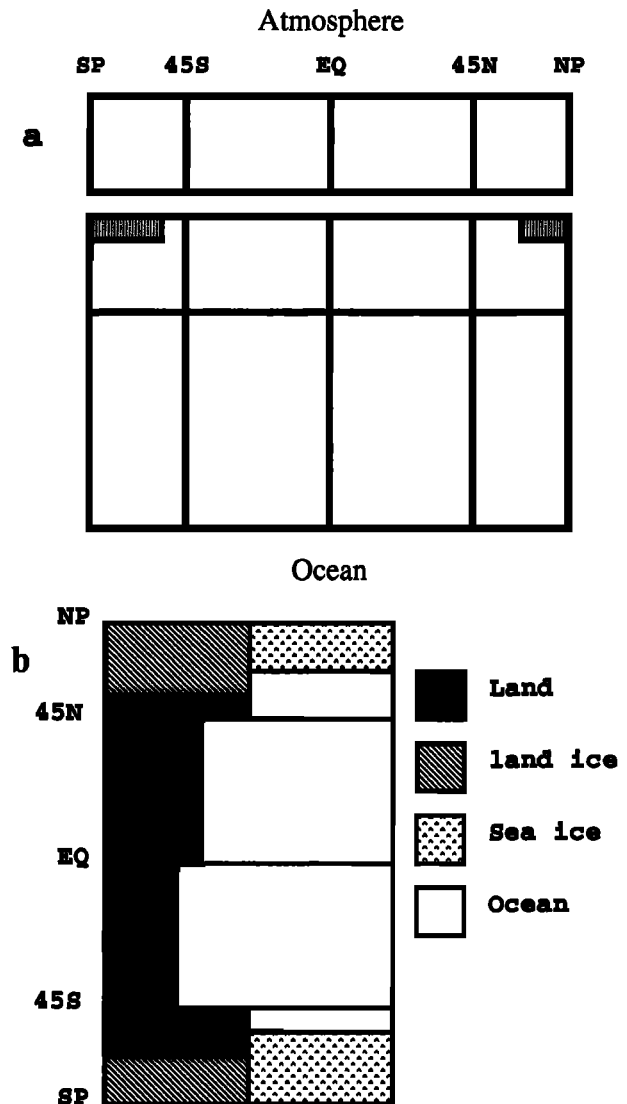


Figure 1. The box model (a) meridional cross section with shaded regions representing sea ice cover and (b) top view.

also includes the Milankovitch variations for each atmospheric box. The Milankovitch forcing also enters in the land glacier ablation term as explained below. The Milankovitch variations in insolation are based on the algorithm and code of Berger [1978]. The transition from annual mean to seasonal and Milankovitch solar forcing required some fairly minor tuning to a very few of the model parameters and these are shown in Table 1. The ocean is represented in our model by four upper ocean boxes and four deep boxes, where the meridional thermohaline circulation is calculated from the meridional density gradients [Stommel, 1961] and is driven by air-sea fluxes of heat and fresh water as well as by freshwater fluxes from land ice ablation and runoff. Sea ice forms when the ocean water temperature decreases below a critical freezing temperature and melts above

Table 1. Modified parameters

Parameter	Annual Experiment	Seasonal Experiment
$\alpha_{\text{Land-ice}}$		0.85
P_{lw1}, \dots, P_{lw4}	0.58, 0.56, 0.54, 0.626	0.66, 0.53, 0.51, 0.72
$LI_{\text{Sink4}}, \text{Sv}$		0.076
r, s^{-1}	$3. \times 10^{-4}$	2.6×10^{-4}
$K_h, \text{m}^2 \text{s}^{-1}$	3.5×10^{-4}	1.5×10^{-4}

that temperature. The sea ice cover is assumed to grow within the southern and northern polar ocean boxes with an initial thickness of 1.5 and 2 m respectively, and then to become thicker if the entire polar box is sea ice covered (the sea ice never fills the entire polar boxes in the simulations presented below). The presence and evolution of sea ice affect the surface albedo, the salinity budget in the ocean, and also the air-sea fluxes (heat flux and evaporation) by partially insulating the ocean from the atmosphere.

The atmospheric model (Figure 1) roughly follows those of *Marotzke and Stone* [1995] and *Rivin and Tziperman* [1997] and is divided into four vertically averaged boxes, representing the same latitude bands as the upper ocean boxes. The lower surface of each atmospheric box is a combination of ocean, land, land ice and sea ice, each with its specified albedo. The averaged potential temperature of each atmospheric box is calculated on the basis of the energy balance of the box, taking into account (1) incoming solar radiation (including the Milankovitch variations) using a box albedo calculated according to the relative fraction of each lower surface type in the box, (2) outgoing long-wave radiation at the top of the atmosphere, (3) heat flux into the ocean, and (4) meridional atmospheric heat transport. The meridional atmospheric moisture transport is proportional to both the meridional atmospheric temperature gradient (setting the strength of the synoptic eddies that carry the eddy meridional moisture flux) and to the humidity of the atmospheric box to which the flux is directed (representing the ability of the atmospheric box receiving the moisture flux to actually hold this moisture and carry it poleward from the common boundary with the midlatitude box toward the land glaciers and polar ocean). This formulation results in an increased meridional transport of humidity during warmer periods, contributing to the temperature-precipitation feedback used by *Källén et al.* [1979], *Ghil et al.* [1987], and *Ghil* [1994]. Another source of snow accumulation over land ice sheets in the polar boxes is due to evaporation from the polar ocean box. Sea ice cover during cold periods reduces this source of moisture [Stokes, 1955; Donn and Ewing, 1966; Rudiman and McIntyre, 1981], thus complementing the temperature-precipitation feedback. Larger accumula-

tion rates in warmer periods, consistent with our model formulation, are seen in many proxy records in both Greenland and Antarctica [Cuffy and Clow, 1997; Alley et al., 1993; Lorius et al., 1985]. For a complete discussion regarding the hydrological cycle, the reader is referred to part 1.

The model for land ice sheets, whose slow evolution provides the 100 kyr timescale in our model, is zonally symmetric and assumes perfect plasticity, so that its height is assumed parabolic in latitude [Weertman, 1976; Ghil, 1994]. The ice sheet grows owing to precipitation in the polar boxes, assumed to be distributed evenly in the box. Ice sheets can decrease as a result of ablation, ice runoff, and calving processes. The temperature dependency of ablation is assumed negligible during the past 900 kyr [Huybrechts et al., 1991; Källén et al., 1979].

In part 1 we used a constant sink term representing ablation in the glacier mass balance equation. Owing to the small effective heat capacity of land/glacier surfaces, summer insolation directly determines the summer temperature of these surfaces. This surface temperature during June, in turn, determines the survival of new snow accumulated during the past winter season and also the melting at the glacier surface. High surface summer temperatures lead to a significant melting of new snow and of the upper glacier mass during the summer season [Held, 1982]. In order to parameterize this effect of the summer Milankovitch forcing a linear sink term proportional to the summer radiation was added to the land ice mass balance equation. This term is, in effect, a linearization of the radiation-dependent melting process. For the northern polar box this term is

$$LI_{\text{Sink}} = CLI + \gamma_{LI}(\text{Solar}_{\text{June}} - \text{Solar}_{\text{ave June}}), \quad (1)$$

where CLI and γ_{LI} are constants ($CLI = 0.087 \text{ Sv}$ and $\gamma_{LI} = 0.00095 \text{ Sv m}^2 \text{ W}^{-1}$) and $\text{Solar}_{\text{June}} - \text{Solar}_{\text{ave June}}$ is the anomaly in summer insolation in this box relative to an average over the past 1,000,000 years.

The above parameterization is linear in the Milankovitch forcing and is therefore expected to induce a linear response in the volume of the land ice sheets at the timescales of 23 kyr and 41 kyr, consistent with the proxy records [Imbrie et al., 1992; Saltzman, 1990].

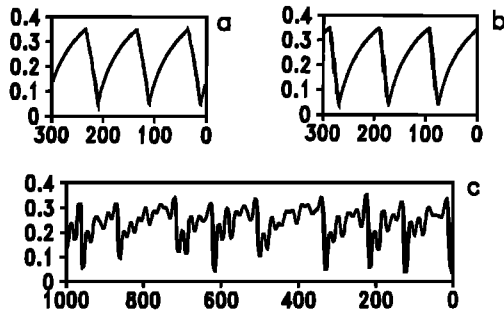


Figure 2. Land ice extensions as a fraction of the northern polar box for (a) annual, (b) seasonal, and (c) Milankovitch model runs.

3. Seasonal Forcing

Figure 2 compares time series of sea ice and land ice extents for the annual model of part 1 (Figure 2a) and for the seasonally forced model (Figure 2b) using present-day orbital parameters from Berger [1978]. Clearly, the glacial oscillation has the same structure and, indeed, the same mechanism with and without the seasonal cycle. The oscillation mechanism was described in detail in part 1, and is now briefly summarized on the basis of the seasonal model results (Figure 3). Starting from an interglacial, as the land ice begins to grow from its minimum point (Figure 3a, year 120,000) the ocean is ice-free (Figure 3b), and the atmospheric and oceanic temperatures in the northern box are rather mild (Figures 3c and 3g). The amount of precipitation enabling glacier growth exceeds the ablation, melting, and calving term (Figure 3f), and therefore the glacier gradually grows. The resulting slow increase in land albedo slowly reduces the temperature of the atmosphere (Figure 3c) and of the ocean (Figure 3g) in the corresponding polar box. When the ocean sea surface temperature (Figure 3g) reaches the critical freezing temperature (year 45,000), sea ice starts to form very rapidly (Figure 3b). The creation of sea ice further increases the albedo, induces a further reduction of atmospheric temperature, and results in the creation of more sea ice (positive feedback). In < 20 years, almost the entire polar box ocean surface is covered by sea ice. Sea ice stops growing when it isolates enough of the ocean from the cold atmosphere, reducing the air-sea cooling that leads to the sea ice formation. At this value of the sea ice cover the sea ice stops growing because there is a balance between the reduced atmospheric cooling of the polar ocean box and the meridional heat transport carried by the thermohaline circulation (THC) toward the same polar ocean box. The sea ice “switch” is now turned to “on.”

At this stage, the average global temperature is at its lowest point, sea ice and land ice sheet extents are maximal, and the system is at a glacial maximum. Be-

cause of the low polar box atmospheric temperature (Figure 3c, year 45,000), there is a large decline in poleward moisture flux, which is about half its maximum value. Similarly, the sea ice cover limits the moisture extraction by evaporation from the polar ocean box and further reduces the corresponding snow accumulation over the land ice. As ablation and glacier runoff proceed as before, being less sensitive to temperature than precipitation, the glaciers start retreating. The land albedo decreases again, and the atmospheric temperature rises slowly. This is the beginning of the termination stage of the glacial period. The upper ocean in the polar box is at the freezing temperature as long as sea ice is present. However, once the deep ocean warmed enough to allow the upper ocean to warm as well, the sea ice melts within ~ 40 years. (Similar rapid retreat of sea ice may have occurred at the end of the Younger Dryas [Dansgaard *et al.*, 1989]). The sea ice switch is now turned to “off,” the temperature of both the atmosphere and the ocean are at their maximum values, and the system is at an interglacial state, having completed a full glacial cycle.

The glacial oscillation in our model is a nonlinear relaxation oscillation. On the basis of the insight we have obtained into the oscillation mechanism, we have formulated a simple argument for the 100 kyr timescale [Gildor and Tziperman, 2000] which we briefly reproduce here. Let the variable part of the land glaciers have a volume ΔV . Assume (closely approximating the solid line in Figure 3f) that the glacier is fed at either a maximum accumulation rate M_{\max} (during an interglacial period) or at a minimum rate M_{\min} and further assume a constant ablation sink rate S . The total timescale of a complete cycle is then

$$\tau = \tau_{\text{buildup}} + \tau_{\text{deglaciation}} = \frac{\Delta V}{(M_{\max} - S)} + \frac{\Delta V}{(S - M_{\min})}.$$

For reasonable choices of the different parameters, one obtains $\tau \approx 100$ kyr, and the minimum of τ as function of the sink amplitude is ~ 50 kyr and occurs for a symmetric oscillation ($\tau_{\text{buildup}} = \tau_{\text{deglaciation}}$), when $S = (M_{\max} + M_{\min})/2$. Note that a straight forward linear timescale gives $\tau_{\text{linear}} = \Delta V/M_{\max} = 10$ kyr only.

While the glacial oscillation mechanism is unchanged from the annually forced model of part 1, the seasonally varying forcing induces seasonal variations in all model variables as shown in Plate 1. Plate 1a shows that during the glacial termination periods, when the sea ice switch is “on,” the sea ice cover undergoes a strong seasonal cycle. Proxy observations [de Vernal *et al.*, 1997; *Climate: Long-Range Investigation, Mapping, and Prediction Project*, 1976; Weinelt *et al.*, 1996] indicate that, indeed, while the winter sea ice cover during the maximum glacial (18 kyr B.P.) was fairly extensive (down to as south as 40° – 45° N), much of

Seasonal forcing

Milankovitch forcing

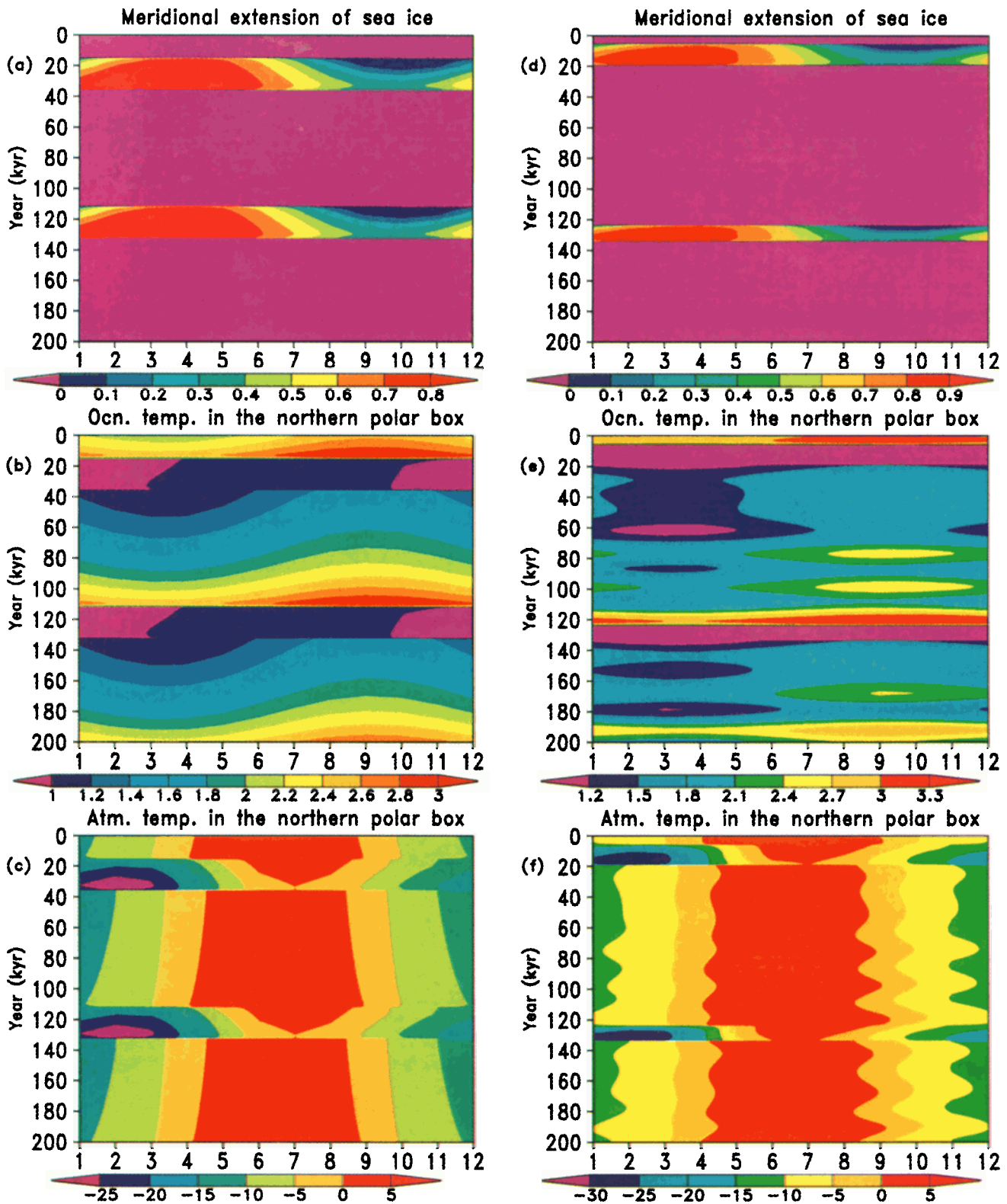


Plate 1. The evolution of seasonal cycle in a few key variables during the glacial cycle for the seasonally forced run (left) and Milankovitch forced run (right) as function of month and time during the glacial cycle. (a,d) Meridional sea ice extension in the northern polar box, (b,e) Sea surface temperature (SST) in the northern polar box ($^{\circ}\text{C}$), and (c,f) atmospheric temperature in the northern polar box ($^{\circ}\text{C}$).

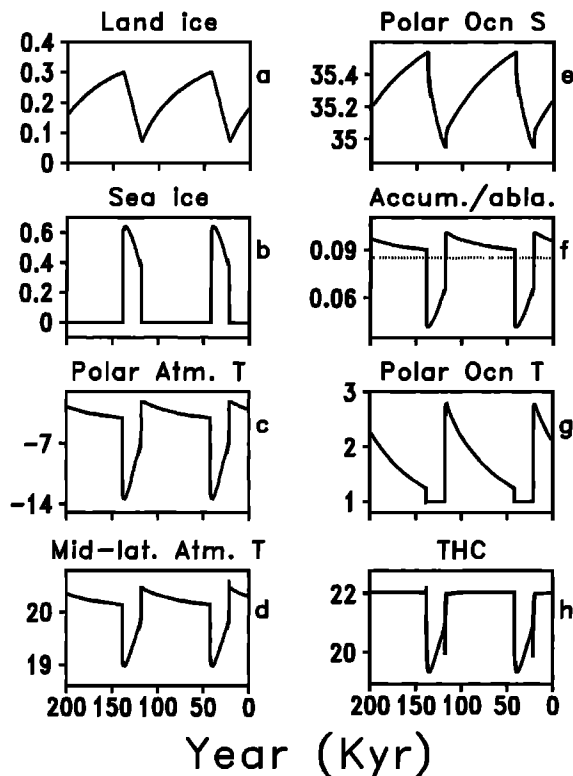


Figure 3. Annual mean results from a seasonally forced model run without Milankovitch forcing, showing (a) northern land ice extent as a fraction of the polar land box area; (b) northern sea ice extent as a fraction of polar ocean box area, (c) northern atmospheric temperature ($^{\circ}\text{C}$), (d) midlatitude atmospheric temperature ($^{\circ}\text{C}$); (e) salinity in the northern upper polar box (ppt), (f) source term (solid line) and sink term (dash line), for northern land glacier ($10^6 \text{m}^3 \text{s}^{-1}$), (g) temperature in the northern upper polar ocean box ($^{\circ}\text{C}$), and (h) Thermohaline circulation (THC) through the northern polar boxes ($10^6 \text{m}^3 \text{s}^{-1}$).

this ocean area was ice-free during the summer months. This is clearly the situation also in our model. In our box model the effects of the sea ice on the moisture source (snow accumulation) for the glaciers (not shown) implies that the moisture source during the glacial termination phase is large during the summer when the sea ice cover is small, and small during the winter months when the sea ice cover is fuller. In reality, however, it is more likely that most of the accumulation over the glaciers occurs due to winter storms. In this, the winter sea ice during the termination phase will act to shut off this source by redirecting the storm track and reducing evaporation from the ocean, while the summer moisture flux will also be small owing to the lack of such storms. This would result in an even more complete shutoff of the moisture source during glacial termination and thus in a yet shorter termination phase than seen in our model.

The existence of sea ice during the termination phase implies in our simple model that the SST in the po-

lar box is at the freezing temperature at that time (Plate 1b). Right after the sea ice switch turns to "off" (116 kyr), a seasonal cycle develops in the SST, and this seasonal cycle is superimposed on the general cooling trend during the slow growth of the land glaciers (116-38 kyr).

The seasonal cycle in the model sea surface salinity (SSS, not shown) is very weak away from the termination phase, and one can only see the general trend in SSS due to the freshwater flux from the ocean to the land glaciers. However, when sea ice is present, its seasonal cycle forces also a seasonal cycle in the SSS via the processes of brine rejection during sea ice freezing and freshwater release during melting.

The seasonal cycle in the midlatitude atmospheric box temperature (not shown) is fairly uniform throughout the glacial-interglacial cycle, apart from a small ($\sim 1^{\circ}$) shift toward colder temperatures during the termination phase when the polar ocean is ice-covered. The evolution of the seasonal cycle amplitude in the northern polar atmospheric box (Plate 1c) is more dramatic because during the termination stage the seasonal cycle of the sea ice induces a larger seasonal cycle in the atmospheric temperature via its albedo effect.

In the southern polar box, sea ice covers most of the ocean surface throughout the year, and the seasonal cycle in sea ice and SST is weaker than it should be during the whole glacial cycle (not shown). The climate signal of the Northern Hemisphere glaciations transferred to the Southern Hemisphere in our model is probably too weak, perhaps owing to the lack of variable global sea level and atmospheric CO_2 concentration in the current version of the model.

4. Milankovitch Forcing

We now proceed to examine the effects of Milankovitch forcing on the glacial cycle in our model. Figure 2c shows a 1 million year time series of Northern Hemisphere land ice volume from a Milankovitch-forced run, showing the same features of an asymmetric sawtooth structure with a roughly 100 kyr timescale, as seen in the annual and seasonal runs (Figures 2a and 2b).

Figure 4 presents an annual mean time series of key model variables for the last 200 kyr period of Milankovitch-forced run. A comparison to Figure 3 for the seasonal run demonstrates that the basic mechanism of the 100 kyr oscillation is unchanged from the annual and seasonal models with no Milankovitch solar variations. The higher frequencies of 41 kyr and 23 kyr are now superimposed on the dominant 100 kyr cycle. These timescales in the land ice sheet come from the Milankovitch-dependent sink term (1) and propagate to other model variables as well.

The results of an experiment in which the Milankovitch solar variability affects only the incoming radiation into each of the atmospheric boxes but does not enter

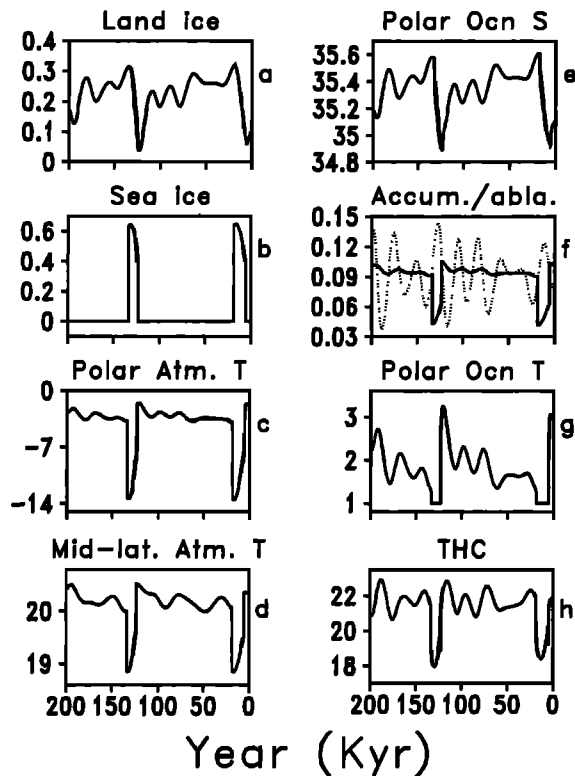


Figure 4. Annual mean results from the Milankovitch-forced seasonal run: same diagnostics as in Figure 3.

the land ice sink term are presented in Figure 5. The 23 and 41 kyr time scales' variability is significantly weaker than that observed in proxy records. The 23 kyr and 41 kyr cycles appear in this model experiment only in variables such as midlatitude atmospheric temperature, which are forced directly by insolation changes. Thus the effect of Milankovitch solar variability on annual mean climate variables is clearly via the mass balance of the land ice sheets rather than by affecting the atmospheric temperature directly.

The seasonal variations of key model parameters during a complete glacial cycle from the Milankovitch-forced run (from 200 kyr B.P. to present day) are shown on the right of Plate 1. Besides the seasonal cycle seen in the seasonally forced case without Milankovitch solar variations (Plate 1, left), a 23 kyr modulation in variables affected directly by solar radiation (e.g., atmospheric temperature (Plate 1f)) can be easily seen. Because of gradual weakening of the 23 kyr amplitude in Milankovitch forcing during the past 50 kyr or so [see, e.g., *Imbrie et al., 1993, Figure 1*], the 23 kyr modulation has a stronger amplitude from 200 kyr to 60 kyr ago than during the past 60 kyr.

Figure 6a shows the power spectra of the northern polar box land ice extension for the annual (dashed line), seasonal (dotted line) and Milankovitch (solid) runs for periods larger than 10 kyr. The model was run using Milankovitch varying solar forcing for six different

initial conditions for the northern polar land ice extension (see below). The spectrum for the Milankovitch runs (solid curve in Figure 6a) is based on an average of these six time series of one million years each, with sampling every 200 years. The seasonal and annual spectra are based on a single one million year time series each. Each spectral estimate was calculated using time series sections of 409,600 years, with a 50% overlap and a Hanning window. Sampling the time series every 10 years leaves the spectra unchanged; the means have been subtracted from all time series prior to calculating the spectra.

Interestingly, the spectral peak at 100 kyr in the Milankovitch forced run is lower and wider than in the seasonal and annual runs. This seems to be because the Milankovitch variations in the solar radiation tend to delay or shorten the occurrence of glacial terminations, depending on the relative phase of the land ice and the Milankovitch forcing (see below). This makes the period of the glacial-interglacial cycle less uniform than in the run without the Milankovitch forcing, hence the weaker and wider 100 kyr peak in Figure 6. Proxy records also show that the interval between terminations is not constant, ranging from 80 to 120 kyr [*Raymo, 1997*].

While the Milankovitch forcing may be too weak at 100 kyr to account for the observed climate signal at this frequency, Milankovitch forcing still affects the characteristics of the 100 kyr cycle through nonlinear phase locking by acting as a pacemaker [*Saltzman et al., 1984; Imbrie et al., 1993*]. Figure 7 shows the land ice sheet extent as a function of time for six Milankovitch-forced runs starting from different initial conditions for the northern polar ice sheet extent, with all other initial conditions, forcing, and model parameters being identical. After a while, all runs converge into a single time series. Figure 8 shows that the agreement between the global ice volume from one of these experiments with the SPECMAP $\delta^{18}\text{O}$ data [*Imbrie et al., 1984*] is quite reasonable.

The model glacial-interglacial oscillation is clearly phase locked to the orbital variations through a nonlinear mechanism [*Ghil, 1994; Saltzman et al., 1984; Paillard, 1998*]. Because the amplitude of the Milankovitch forcing in a given frequency band changes with time

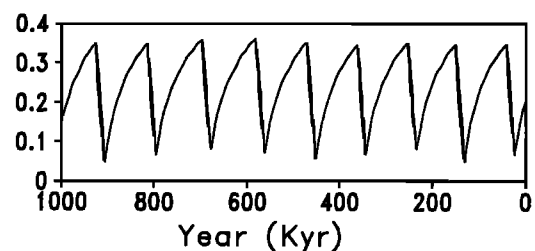


Figure 5. Land ice extent from a run with Milankovitch forcing included only in the incoming solar radiation but not in the glacier ablation/sink term.

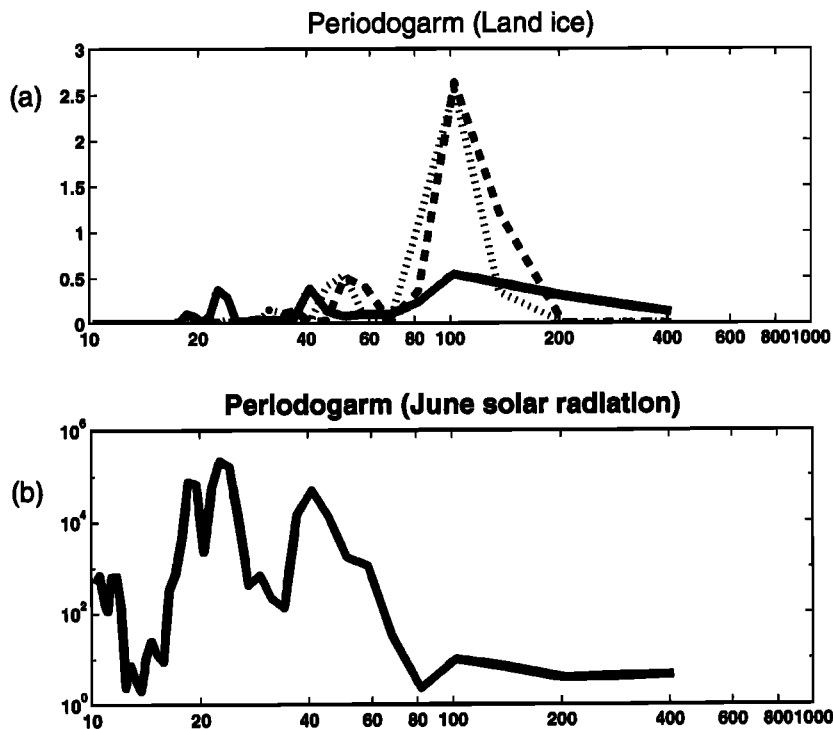


Figure 6. (a) Power spectrum of land ice extension variation in the Milankovitch run (solid line), annual run (dashed line), and seasonal run (dotted line). (b) Power spectrum of June solar radiation in northern polar box.

[Imbrie *et al.*, 1993], it is not possible in the present model to clearly indicate which of the Milankovitch frequencies (or which combination of these forcing frequencies) is responsible for the phase locking of the 100 kyr cycle. This is in contrast to the alternative mechanism of Ghil and colleagues [Källén and Ghil, 1979; Le Treut and Ghil, 1983] in which a specific combination of Milankovitch frequencies of 19 and 23 kyr is proposed to be responsible for the 100 kyr glacial oscillation.

Glacial terminations in our model start when the sea ice switch is on, whenever the ocean temperature decreases to the critical freezing temperature. Several mechanisms may lead to such a cooling. One is a lower northern summer insolation (due to Milankovitch variations). Another mechanism, more dominant in the en-

ergy balance of the northern atmospheric polar box of our model and hence in setting the ocean temperature, is the land ice sheet through its albedo effect. This is consistent with the finding of Felzer *et al.* [1996] based on a GCM study.

This dominance of the ice sheet albedo effect in the energy balance of the atmospheric boxes leads to a specific physical mechanism for the phase locking of the glacial oscillation to the Milankovitch insolation variations. When the ice sheet has matured and its albedo has cooled the climate significantly, the SST is not far from its freezing point. At this stage a relatively small

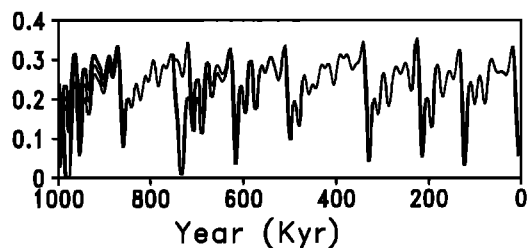


Figure 7. Six model runs forced by Milankovitch forcing and starting from different initial extensions of the northern box land ice.

SPECMAP Vs. MODEL

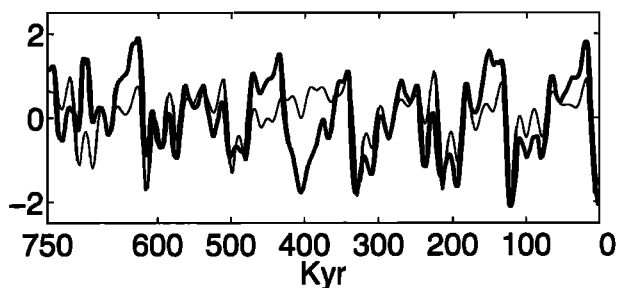


Figure 8. Comparison between the (normalized) global ice volume from the model run (thin line) and SPECMAP $\delta^{18}O$ curve (thick line).

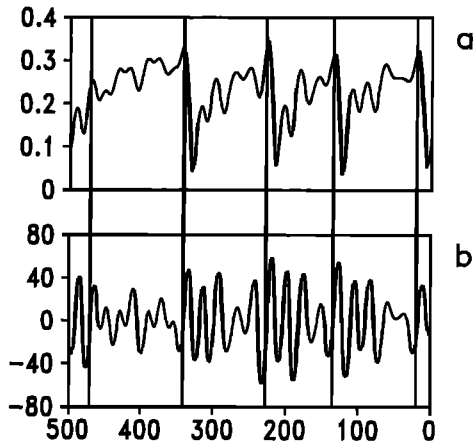


Figure 9. Model land ice and June solar radiation anomaly for the last 400 kyr showing the tendency of deglaciations to initiate during low Milankovitch solar radiation phase.

reduction in rate of ablation due to Milankovitch insolation changes leads to further glacier growth; this can induce the small cooling needed for the development of a sea ice cover and thus lead to an early glacial termination. Similarly, a high insolation and therefore high ablation can reduce the ice sheet extent and delay the sea ice growth and the deglaciation. This insight also leads to a prediction, based on our model results, of the expected relative phase of Milankovitch forcing and the glacial terminations. That is, we expect the sea ice switch to turn to on and a deglaciation to begin when the Milankovitch insolation in the Northern Hemisphere is at a low phase. This is consistent with the suggestion of *Raymo* [1997], based on various proxies, that glacial terminations start during cold summers induced by the Milankovitch forcing. Figure 9 shows that, indeed, in our model the onset of glacial terminations (Figure 9a) tends to occur during a cold summer phase of the Milankovitch forcing (Figure 9b).

Finally, let us consider the transition from a 41 kyr glacial cycle to a 100 kyr glacial oscillation about one million years ago [*Ruddiman and Raymo, 1988*]. It has been suggested that this change was induced by a general cooling due to a slow CO_2 decline due to tectonic activity [*Raymo, 1998; Saltzman, 1987; Saltzman and Verbitsky, 1994; Maasch and Saltzman, 1990*] or by a gradual increase of the total ice sheet volume [*Ghil and Childress, 1987*]. Our sea ice switch mechanism can incorporate such a scenario, as follows.

We assume that prior to the climate transition of one million years ago the warmer climate did not allow for a significant sea ice cover to develop. As a result, the sea ice switch mechanism was deactivated, and glacial oscillations were only the result of the linear forcing of the Milankovitch variability affecting the land ice sink term (1). Then, at about 700 kyr ago, the slow climate

cooling for one of the reasons mentioned above allowed the sea ice cover to expand more substantially. This allowed the sea ice to exert a more significant influence on the hydrological cycle and on moisture extraction from the polar ocean and started the 100 kyr oscillation described above. Figure 10 shows the northern land ice extent in a model run for the past 1.4 million years under Milankovitch forcing, in which we have restricted the sea ice cover to 0.05 of the northern polar box until 700 kyr ago and then let it vary freely. The results indeed show that the oscillation was dominated by the 23 and 41 kyr frequencies prior to the activation of the sea ice switch. This model time series is roughly similar to proxy records from the early Pleistocene period [*Prentice and Matthews, 1988*] and serves as another indication that the sea ice switch mechanism may indeed play a significant role in the glacial dynamics as well as in the climate transition of around 700 kyr ago.

5. Conclusion

In this paper we have examined the interaction of the 100 kyr glacial oscillation due to the sea ice switch mechanism [*Gildor and Tziperman 2000*] with seasonal and Milankovitch forcing. In the work of *Gildor and Tziperman* [2000], referred to as part 1 throughout the text, the analysis of this sea ice switch mechanism of the glacial-interglacial oscillations has led to the development of a heuristic argument for the 100 kyr timescale which was also briefly described in section 3. Part 1 also analyzed the sensitivity of this oscillation to various model parameters and has extensively discussed the robustness of the model results in view of the coarse resolution of our box model; it should be noted that this model, while simple, is still significantly more detailed than previous models applied to the same problem. *Gildor and Tziperman* [2000] have also discussed quite extensively the agreement and disagreement between various proxy data sets and the model results. We briefly note here that our model predicts that the onset of the land deglaciation should correspond to a larger sea ice cover, and hence a colder period. Indeed, *Bard et al.* [1996] showed evidence that a freshwater

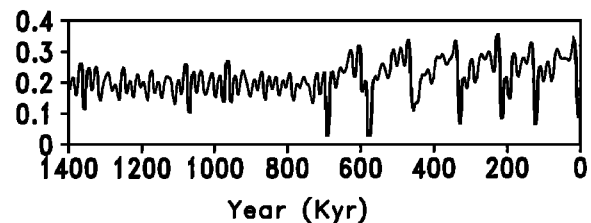


Figure 10. Model northern land ice extent for a run emulating the transition from the warmer climate of the early Pleistocene period over 700 kyr ago by limiting the sea ice cover to 0.05 of the polar boxes area until 700 kyr, when the sea ice is made free to evolve.

pulse due to land deglaciation seem to have occurred within a *cold* event that followed the initiation of the Bølling/ Allerød warm period. The interested reader is referred to part 1 for additional details.

The oscillation's mechanism, timescale, and asymmetric sawtooth shape were shown in this paper to remain basically the same in the presence of the seasonal and Milankovitch variations in the solar radiation. Still, we have shown that the Milankovitch forcing plays an important role in linearly forcing the 23 and 41 kyr climate responses through the control of land ice melting by the Northern Hemisphere summer radiation. These frequencies, in turn, were shown in our model to phase lock the 100 kyr glacial-interglacial oscillation [Saltzman et al., 1984; Paillard, 1998]. The phase-locked model simulation of the land ice extent compares favorably with the SPECMAP time series.

On the basis of our model results we have given a simple argument according to which the onset of glacial terminations needs to occur during cold summers, induced by Milankovitch cold summer insolation, consistent with the data analysis of Raymo [1997]. We have also shown that the presence of Milankovitch forcing and its effect on the onset of glacial terminations induced a variable period of the glacial-interglacial oscillation. This variable period induces a widening and weakening the spectral peak of the 100 kyr oscillation relative to the model runs without Milankovitch forcing. Our heuristic explanation for the 100 kyr timescale, which is based on our understanding of the sea ice switch mechanism (section 3), is based on an assumed constant glacier ablation sink term. In the presence of Milankovitch variations the sink term is no longer constant, leading to the observed changes in the glacial-interglacial timescale.

We have also examined the seasonal variation in the various model variables, such as oceanic and atmospheric temperatures and sea ice cover as well as the changes in the seasonal cycle during different phases of the 100 kyr cycle. The generally reasonable ampli-

tude we find for the model seasonal cycle enhances the confidence in the model results. More specifically, the existence of a seasonal cycle in sea ice cover even during the glacial cycle makes the model simulation consistent with proxy records (such as of biological productivity) that indicate that sea ice cover was indeed seasonal over much of the northern North Atlantic [de Vernal et al., 1997; Weinelt et al., 1996].

A most interesting consequence of including Milankovitch forcing in the model simulation is a resulting possible explanation of the climate transition about 700 kyr ago from a 41 kyr oscillation to a 100 kyr oscillation. We have shown that such a transition could result from the activation of the sea ice switch by the general climate cooling during that period due to either a tectonically induced reduction in CO₂ concentration [Raymo, 1998; Ruddiman and Raymo, 1988; Maasch and Saltzman, 1990] or a gradual increase in land ice volume [Ghil and Childress, 1987].

While the model used here is fairly idealized, its representation of the various climate components is sufficiently explicit that it makes certain predictions that can be tested with fuller GCMs and possibly with further analysis of proxy records of sea ice as these become available in the future. It would be especially interesting to examine the robustness of the sea ice switch control over the hydrological cycle using an atmospheric GCM as well as the robustness of the rapid sea ice growth using a coupled ocean-sea ice model. It would also be interesting to extract from sea ice proxies that may become available in the future the relative timing of the maximum sea ice cover relative to the timing of the initiation of the land ice deglaciation period as compared to the model scenario presented here.

Acknowledgments. We thank Michael Ghil, Isaac Held, Aldo Shemesh, and Robbie Toggweiler for numerous most useful discussions. We also thank A. Berger for generously providing us with the code for calculating the Milankovitch solar variations. This work is partially supported by the Israeli-U.S. Binational Science Foundation.

References

- Alley, R. B., et al., Abrupt increase in Greenland snow accumulation at the end of the Younger Dryas event, *Nature*, **362**, 527–529, 1993.
- Bard, E., B. Hamelin, M. Arnold, L. Montagnoni, G. Cabioch, G. Faure, and F. Rougerie, Deglacial sea level record from Tahiti corals and the timing of global meltwater discharge, *Nature*, **382**, 241–244, 1996.
- Berger, A., Long-term variations of daily insolation and quaternary climate changes, *J. Atmos. Sci.*, **35**, 2362–2367, 1978.
- Birchfield, E., and M. Ghil, Climate evolution in the Pliocene and Pleistocene from marine-sediment records and simulations: Internal variability versus orbital forcing, *J. Geophys. Res.*, **98**, 10385–10399, 1993.
- Climate: Long-Range Investigation, Mapping, and Prediction Project, The surface of the ice-age Earth, *Science*, **191**, 1131–1136, 1976.
- Cuffy, K., and G. Clow, Temperature, accumulation, and ice sheet elevation in central Greenland through the last deglacial transition, *J. Geophys. Res.*, **102**, 26,383–26,396, 1997.
- Dansgaard, W., J. White, and S. Johnsen, The abrupt termination of the Younger Dryas climate event, *Nature*, **339**, 532–534, 1989.
- de Vernal, A., et al., Sea-surface conditions in the northwest North Atlantic during the Last Glacial Maximum, *GEOTOP Contrib.*, **97-001**, Res. Cent. in Isotopes Geochem. and Geochron., Montreal, Quebec, Canada, 1997.
- Donn, W., and M. Ewing, A theory of ice age III, *Science*, **152**, 1706–1712, 1966.
- Felzer, B., R. Oglesby, T. Webb III, and D. E. Hyman, Sensitivity of a general circulation model to changes in Northern Hemisphere ice sheets, *J. Geophys. Res.*, **101**, 19,077–19,092, 1996.
- Ghil, M., Cryothermodynamics: The chaotic dynamics of paleoclimate, *Physica D*, **77**, 130–159, 1994.
- Ghil, M., and S. Childress, *Topics in Geophysical Fluid Dynamics: Atmospheric*

- Dynamics, Dynamo Theory and Climate Dynamics*, Springer-Verlag, New York, 1987.
- Ghil, M., and H. Le Treut, A climate model with cryodynamics and geodynamics, *J. Geophys. Res.*, **86**, 5262–5270, 1981.
- Ghil, M., A. Mullhaupt, and P. Pestiaux, Deep water formation and Quaternary glaciations, *Clim. Dyn.*, **2**, 1–10, 1987.
- Gildor, H., and E. Tziperman, A sea ice climate switch mechanism for the 100 kyr cycles, *J. Geophys. Res.*, in press, 2000.
- Held, I., Climate models and the astromical theory of ice age, *Icarus*, **50**, 449–461, 1982.
- Huybrechts, P., A. Letreguilly, and N. Reeh, The Greenland ice sheet and greenhouse warming, *Paleogeogr., Paleoclimatol., Paleocol.*, **89**, 399–412, 1991.
- Imbrie, J., J. Hays, D. Martinson, A. McIntyre, A. Mix, J. Morley, N. Pisias, W. Prell, and N. Shackleton, The orbital theory of Pleistocene climate: Support from a revised chronology of the marine $\delta^{18}\text{O}$ record, in *Milankovitch and Climate, Part I*, pp. 269–305. D. Reidel, Norwell, Mass., 1984.
- Imbrie, J., et al., On the structure and origin of major glaciation cycles, 1, Linear responses to Milankovitch forcing, *Paleoceanography*, **7**, 701–738, 1992.
- Imbrie, J., et al., On the structure and origin of major glaciation cycles, 2, The 100,000-year cycle, *Paleoceanography*, **8**, 699–735, 1993.
- Källén, E., C. Crafoord, and M. Ghil, Free oscillations in a climate model with ice-sheet dynamics, *J. Atmos. Sci.*, **36**, 2292–2303, 1979.
- Le Treut, H., and M. Ghil, Orbital forcing, climatic interactions, and glaciation cycles, *J. Geophys. Res.*, **88**, 5167–5190, 1983.
- Lorius, C., J. Jouzel, C. Ritz, L. Merlivat, N. Barkov, Y. Korotkevich, and V. Kotlyakov, A 150,000-year climatic record from Antarctic ice, *Nature*, **316**, 591–596, 1985.
- Maasch, K., and B. Saltzman, A low-order dynamical model of global climatic variability over the full Pleistocene, *J. Geophys. Res.*, **95**, 1955–1963, 1990.
- Marotzke, T., and P. H. Stone, Atmospheric transports, the thermohaline circulation, and flux adjustments in a simple coupled model, *J. Phys. Oceanogr.*, **25**, 1350–1364, 1995.
- Milankovitch, M., *Mathematische Klimalehre und Astromoische Theorie der Klimaschwankungen I*, *Handbuch der Klimatologie, Part A*, Verlag Borntrager, Berlin, Germany, 1930.
- Paillard, D., The timing of Pleistocene glaciations from a simple multiple-state climate model, *Nature*, **391**, 378–381, 1998.
- Prentice, M., and R. Matthews, Cenozoic ice-volume history: Development of a composite oxygen isotope record, *Geology*, **16**, 963–966, 1988.
- Raymo, M. E., The timing of major terminations, *Paleoceanography*, **12**, 577–585, 1997.
- Raymo, M. E., Glacial puzzles, *Science*, **281**, 1467–1468, 1998.
- Rivin, I., and E. Tziperman, Linear versus self-sustained interdecadal thermohaline variability in a coupled box model, *J. Phys. Oceanogr.*, **27**, 1216–1232, 1997.
- Ruddiman, W. F., and A. McIntyre, Oceanic mechanisms for amplification of the 23,000-year ice-volume cycle, *Science*, **212**, 617–627, 1981.
- Ruddiman, W., and M. E. Raymo, Northern Hemisphere climate regimes during the past 3 Ma: Possible tectonic connections, *Philos. Trans. R. Soc. London, Ser. B*, **318**, 411–430, 1988.
- Saltzman, B., Carbon dioxide and the $\delta^{18}\text{O}$ record of late-Quaternary climatic change: A global model, *Clim. Dyn.*, **1**, 77–85, 1987.
- Saltzman, B., Three basic problems of paleoclimatic modeling: a personal perspective and review, *Clim. Dyn.*, **5**, 67–78, 1990.
- Saltzman, B., and M. Verbitsky, Late Pleistocene climatic trajectory in the phase space of global ice, ocean state, and CO_2 : Observations and theory, *Paleoceanography*, **9**, 767–779, 1994.
- Saltzman, B., A. Hansen, and K. Maasch, The late Quaternary glaciations as the response of a three-component feedback system to Earth-orbital forcing, *J. Atmos. Sci.*, **41**, 3380–3389, 1984.
- Stokes, W. L., Another look at the ice age, *Science*, **122**, 815–821, 1955.
- Stommel, H., Thermohaline convection with two stable regimes of flow, *Tellus*, **13**, 224–230, 1961.
- Weertman, J., Milankovitch solar radiation variations and ice age ice sheet sizes, *Nature*, **261**, 17–20, 1976.
- Weinelt, M., M. Sarnthein, U. Pfauermann, H. Schultz, S. Jung, and H. Erlenkeuser, Ice-free Nordic seas during the last glacial maximum? Potential sites of deepwater formation, *Paleoclimates*, **1**, 282–309, 1996.

H. Gildor and E. Tziperman, Environmental Sciences, Weizmann Institute of Science, Rehovot, 76100, ISRAEL. (e-mail: hezi.gildor@weizmann.ac.il; eli@beach.weizmann.ac.il).

(Received September 27, 1999;
revised June 20, 2000;
accepted July 25, 2000.)